J Mater Sci (2007) 42:2216–2221
DOI 10.1007/s10853-006-1320-0

4TH BRAZILIAN MRS MEETING

Decay of photo-excited conductivity of Er-doped SnO_2 thin films

Evandro A. Morais · Luis V. A. Scalvi

Received: 23 November 2005 / Accepted: 14 February 2006 / Published online: 23 January 2007

Abstract Er-doped SnO_2 thin films, obtained by sol-gel-dip-coating technique, were submitted to excitation with the 4th harmonic of a Nd:YAG laser (266 nm), at low temperature, and a conductivity decay is observed when the illumination is removed. This decay is modeled by considering a thermally activated cross section of an Er-related trapping center. Besides, grain boundary scattering is considered as dominant for electronic mobility. X-ray diffraction data show a characteristic profile of nanoscopic crystallite material (grain average size ≈5 nm) in agreement with this model. Temperature dependent and concentration dependent decays are measured and the capture barrier is evaluated from the model, yielding 100 meV for SnO_2:0.1% Er and 148 meV for SnO_2:4% Er.

Introduction

Doping semiconductors with rare-earth ions may contribute for technological innovation, giving rise to new optoelectronic devices. Er^{3+} is one of the most attractive rare-earth ions for applications, since has one of its luminescent core transitions at 1.54 μm, coincident with the minimum absorption of silica-based optical fibers [1]. A significant loss of photoluminescence (PL) intensity is observed when temperature is raised, bringing down the efficiency for technological application, however the PL quenching decreases with the bandgap energy [2], making rare-earth doping of wide bandgap semiconductors a very attractive process [3]. Besides, these semiconductors present higher excitonic ionization energy, being more efficient matrix to promoting electrically activated emission [4]. Auger processes are also reduced in wide bandgap semiconductors, and Er emission may become a very efficient process close to room temperature [5]. SnO_2 (tin dioxide) is a wide bandgap semiconductor (3.5–4.0 eV) [6, 7], characterized by high *n*-type electrical conductivity, transparency about 90% in the visible and high reflectivity in the infrared [8], being a very promising matrix for potential rare-earth devices. The combination of electro-optical properties of SnO_2 and Er^{3+} luminescent properties may give birth to optical communication devices, such as waveguides [9], optical amplifiers and electroluminescent emitters, operating from visible to infrared.

In order to use Er-doped SnO_2 as active layers in electroluminescent devices, the knowledge of photo-induced electrical properties becomes essential. In the undoped form, SnO_2 is an *n*-type semiconductor, where the negative charge carriers come from oxygen vacancies and interstitial tin atoms, which act as donors in this material. Since Er^{3+} exhibits an acceptor like behavior in tin dioxide [10], Er-doped SnO_2 presents a high degree of electrical charge compensation, leading to high resistivity films. Recent investigations [11] of carrier transport phenomena, above room temperature, in these films, lead to two linear regions of the

E. A. Morais · L. V. A. Scalvi (✉)
Departmento de Fisica – FC, UNESP – Universidade Estadual Paulista, Caixa Postal 473, 17033–360 Bauru, SP, Brazil
e-mail: scalvi@fc.unesp.br

E. A. Morais
Programa de Pós-Graduação em Ciência e Tecnologia de Materiais, UNESP, Bauru, SP, Brazil

plot of current density as function of applied bias. Each of these regions was identified as dominated by a distinct conduction mechanism: Schottky emission for lower applied electric fields and Poole–Frenkel emission for higher fields [12, 13].

The recombination of electron-hole pairs with desorbed oxygen species leads to persistent photoconductivity (PPC) effect in undoped SnO_2 sol-gel thin films [10]. This result may be summarized as the increase of conductivity by illumination with the 4th harmonic of a Nd:YAG laser (266 nm), at low temperature, until saturation, followed by maintenance of the highly conductive metastable state after removing the laser irradiation. The same experiment carried out on Er-doped SnO_2 thin films gives rise to exponential like decay when illumination is removed, instead of the observed PPC for undoped tin dioxide.

The decay of photo-excited conductivity, measurement explored in this paper, was used before in order to understand the electron trapping phenomena and the ground state charge of the dominant defect in other semiconductor materials [14, 15]. From its analysis it is possible to evaluate the time-temperature dependence of charge carrier trapping by the defect and to obtain its thermally activated capture cross section. In this paper we present results of photo-induced thermally dependent conductivity decay for Er-doped SnO_2 thin films doped with distinct Er concentration, deposited by sol-gel-dip-coating (SGDC) process. An analysis of the trapping mechanism by Er-like centers is also presented, allowing the evaluation of the capture cross section of these defects.

Experimental

Starting solutions were prepared by sol-gel process according to procedure described in a recent publication [11]. The desired amount of $ErCl_3{\cdot}6H_2O$ was added to an aqueous solution of $SnCl_4{\cdot}5H_2O$ (0.2 mol l^{-1}), under magnetic stirring, followed by addition of NH_4OH until pH reaches 11. The obtained suspension was submitted to dialysis against distilled water by approximately 10 days in order to eliminate Cl^- and NH_4^+ ions. Previously to the preparation of the thin film, starting solution was concentrated through evaporation of 70% (in volume) of solvent. Films were deposited on silicate glass substrates by dip-coating with 10 cm/min dip rate. Multi-dipped films were continuously deposited at room temperature with a little interruption after each dip, in order to fire the film at 400 °C for 10 min. When the number of layers reached 10, resulting film was annealed at 550 °C for 1 h. The resulting thickness evaluated from scanning electron microscopy was about 210 nm.

Electrical transport measurements become possible by the deposition of Sn electrodes on the samples through a shadow mask in an Edwards evaporator system. Electrodes are annealed to 200 °C by 20 min at room atmosphere. Low temperature electrical measurements were done in a He-closed cycle Janis Cryostat that controls temperature in the range 10–300 K within 0.05 K of precision. For the decay of photo-induced conductivity measurements, samples were irradiated with the 4th harmonic (266 nm) of a Nd:YAG pulsed laser, with 4.8 mJ of energy and 10 Hz of pulse frequency. The illumination lasts 10 min, keeping constant temperature.

For X-ray diffraction measurements it was used a Rigaku diffractometer coupled with a Cu source of 40 kV and 20 mA of current. Detector rate is 0.5° per minute with a 0.02° step.

Analyses of the decay of photoinduced conductivity

When the film is illuminated with the laser source, at low temperature, a sharp increase in the electrical conductivity is observed. Removing the illumination, a decay of conductivity as function of time is observed, which means a sample resistance increase with time. This time-dependent resistance can be given by:

$$R(t) = (K_s \cdot n(t) \cdot \mu.q)^{-1} \tag{1}$$

where K_s is the proportionality constant between conductivity and conductance (form factor), $n(t)$ is the time-dependent electron concentration, μ is the film mobility and q is the electron charge. The decay of photo-induced electrons from the conduction band to the trapping defect is given by [14]:

$$\frac{dn}{dt} = -V_{th} \cdot \gamma_n \cdot n \cdot N_{Def}^{+} \tag{2}$$

where V_{th} is the thermal velocity of free electrons $[(3\ kT/m^*)^{1/2}]$, γ_n is the thermally activated capture cross section and N_{Def}^{+} is the number of ionized defects. Supposing that the Er center is singly ionized, then $N_{Def}^{o} \rightarrow e^- + N_{Def}^{+}$ and then $N_{Def}^{+} = n$, where it is considered that decay time is long enough to neglect electron-hole recombination. γ_n is given by [14]:

$$\gamma_n = \gamma_\infty \cdot \exp\left(-\frac{E_{cap}}{kT}\right) \tag{3}$$

where γ_∞ is the constant capture cross section (infinite temperature) and E_{cap} is the potential barrier for electron trapping by Er^{3+} centers. The solution of Eq. (2) is given by:

$$n(t) = \frac{n(0)}{[1 + n(0) \cdot C_1 \cdot t]} \tag{4}$$

where $C_1 = V_{th} \cdot \gamma_n$ Considering that mobility is dominated by the grain boundary scattering, we may neglect bulk scattering mechanisms (phonon and ionized impurity). The mobility due to grain boundary scattering is given by [16]:

$$\mu = A \cdot T^{-\frac{1}{2}} \cdot \exp\left(-\frac{\phi}{kT}\right) \tag{5}$$

where A is a constant and ϕ is the grain boundary potential barrier for scattering. Zhang and Ma [17], in a review paper, give a value of 30 meV for ϕ, and then, this value will be adopted hereafter in our calculation. Substituting Eqs. (4) and (5) into Eq. (1), one obtains:

$$R(t) = \frac{T^{\frac{1}{2}} \cdot \exp\left(\frac{\phi}{kT}\right) \cdot [1 + n(0) \cdot C_1 \cdot t]}{K_s \cdot A \cdot q \cdot n(0)} \tag{6}$$

which means that $R(t)$ must be a linear function of time for a preset temperature. Evaluating the first derivative and calling it as slope, we get:

$$\frac{dR}{dt} = \text{slope} = K_f \cdot T \cdot \exp\left[-\frac{E_{cap} - \phi}{kT}\right] \tag{7}$$

where K_f is $[\gamma_\infty \cdot (3\ k/m^*)^{1/2} \cdot (K_s \cdot A \cdot q)^{-1}]$ Therefore a plot of ln (slope/T) as function of $1/T$ yields the quantity (E_{cap}–ϕ) directly from the curve inclination.

Results and discussion

Normalized conductivity as function of time is shown in Fig. 1 for Er-doped SnO_2 with 4% Er (1a) and 0.1% Er (1b). As it can be observed, as the temperature increases the decay becomes faster, for the same Er-doping concentration. Comparing both data set, it can be observed that the decay rate becomes slower for the lower Er concentration.

A plot of resistance as function of time is shown in Fig. 2, where the linear nature of the curve for shorter times is clearly observed. Considering that the decay is faster for the more doped film as shown in Fig. 1, we plot the resistance variation in the range 0–20 s for SnO_2:0.1% Er and 0–10 s for SnO_2:4% Er, in Fig. 2.

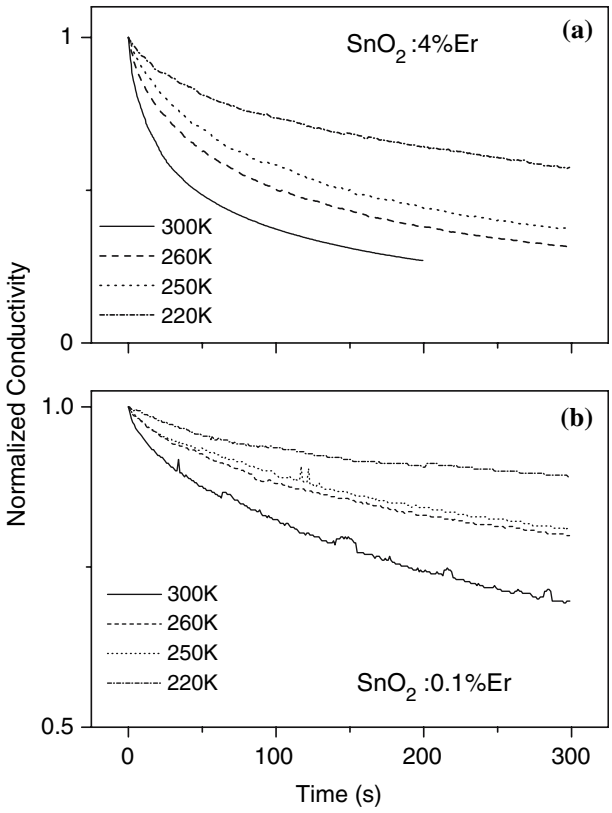

Fig. 1 Decay of photo-excited conductivity at several temperatures for (**a**) SnO_2:4% Er thin film, (**b**) SnO_2:0.1% Er thin film

For longer times, other trapping centers may also begin the competition for electron capture, and a rather distinct free carrier decay rate is expected. Then we have decided to use the initial linear portion of the curve. As clearly seen in Fig. 2, this option is adequate, since very low deviation from the linear behavior is observed. The most clearly observed deviation from linear shape is for SnO_2:0.1% Er at 300 K where a possible electron-hole recombination at the very beginning of conductivity decay may be taking place.

Figure 3 shows resistivity as function of temperature for SnO_2:0.1% Er thin film. The inferior inset is the Arrhenius plot of these data, yielding activation energy of 73 meV for the deepest level, which becomes ionized for higher temperatures. Following the general theory presented in Section ''Analyses of the decay of photoinduced conductivity'', a plot of the slope of $R \times$ time curves as function of temperature in accordance with Eq. (7) is shown in the superior inset of Fig. 3. As already mentioned, the inclination of this plot yields the quantity (E_{cap}–ϕ). For the SnO_2:0.1% Er, shown in the figure, (E_{cap}–ϕ) = 70 meV, which means E_{cap} = 100 meV, since ϕ = 30 meV [17]. A similar procedure for the sample SnO_2:4% Er (not shown) yields (E_{cap}–ϕ) = 118 meV and E_{cap} = 148 meV.

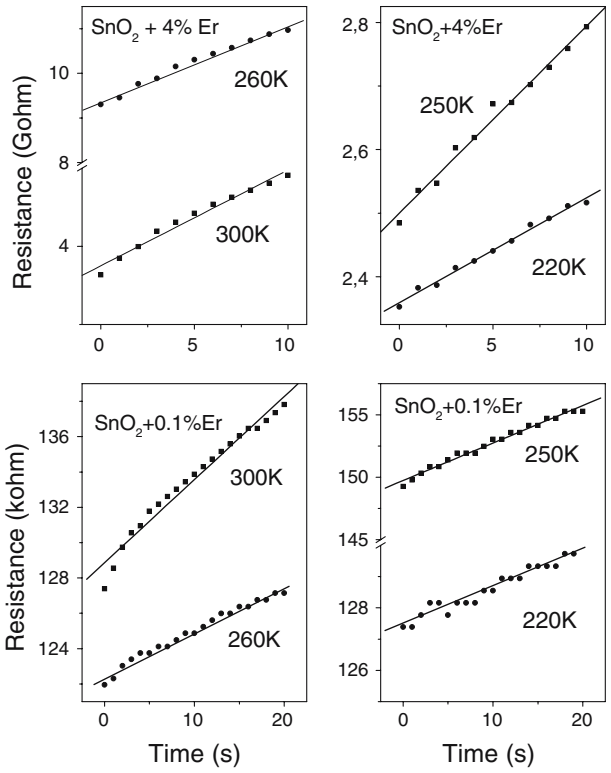

Fig. 2 Resistance as function of time for SnO_2:4% Er and SnO_2:0.1% Er thin films at several temperatures. Full lines—linear data fitting

Unfortunately a plot of resistivity as function of temperature for the same range of Fig. 3 is not possible for SnO_2:4% Er, since the order of magnitude of resistivity may be as high as 10^6 ohm cm at room temperature [11], which makes very difficult to measure it below room temperature. This high resistivity behavior may be related mainly to charge compensation, since undoped SnO_2 presents *n*-type conduction and the increase in the Er-doping concentration induces more electron trapping by Er-related centers. These defects are located either at Sn^{4+} substitutional sites of SnO_2 lattice as well as at grain boundary layer [18], since the solubility limit has been widely overcome for 4% Er-doping. Then, it is not possible to obtain the activation energy for SnO_2:4% Er by an Arrhenius plot. However it is very interesting to notice the agreement between $(E_{cap}–\phi) = 70$ meV and the activation energy (E_a) obtained from the Arrhenius plot ($E_a = 73$ meV) for SnO_2:0.1% Er. This result means that the activation energy obtained from the conventional procedure through Arrhenius plot may be incorrect for materials with nanoscopic grains, because the potential barrier at grain boundary (ϕ) becomes comparable to the thermally activated capture barrier (E_{cap}). Another worthy noting feature of these results is the higher $(E_{cap}–\phi)$ quantity for the more doped sample. Considering that 4% Er-doping means a highly compensated sample (in agreement with the much higher value of resistance—Fig. 2), the increase in conductivity due to laser irradiation is not as large as observed for lower compensated sample. Then, the film of SnO_2:0.1% Er may be considered as a completely degenerated semiconductor in the photo-induced metastable state. In this case, the Fermi level is located above the conduction band edge after laser irradiation, what decreases the effective electron capture barrier. Besides, the value of 30 meV, given by Zhang and Ma [17], for the potential barrier at grain boundary may not be valid for any doping concentration. Moreover, since 0.1% Er is a very close value to solubility-limit, the excess of Er is mainly located at grain boundary surface as we have concluded previously [18]. Then, the time–temperature conductivity decay observed in Fig. 1 corresponds to capture by two different dominant trapping centers: substitutional Er^{3+} at Sn^{4+} sites for SnO_2:0.1% Er and Er^{3+} at grain boundary for SnO_2:4% Er, where very complex centers may be forming since the amount of Er has largely exceeded the solubility limit and then the Er concentration at grain boundary is very large. Anyhow these possibilities are related, since the higher Er concentration at grain boundary must also increase the potential barrier at grain interface, decreasing the mobility.

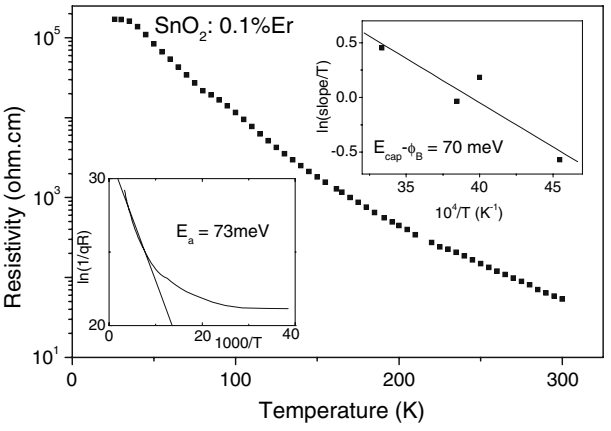

Fig. 3 Resistivity as function of temperature for SnO_2:0.1% Er thin film. Inferior inset—Arrhenius plot of resistivity data, showing the deepest level, ionized at higher temperature range. Superior inset—plot of ln(slope/*T*) as function of reciprocal temperature, according to theory developed in this paper

Figure 4 shows X-ray diffraction data for undoped [19] and Er-doped SnO_2 thin films. It is clearly observed that the most evident peaks are from (110), (101) and (211) which are in good agreement with the cassiterite type structure [20] and exhibits a diffuse

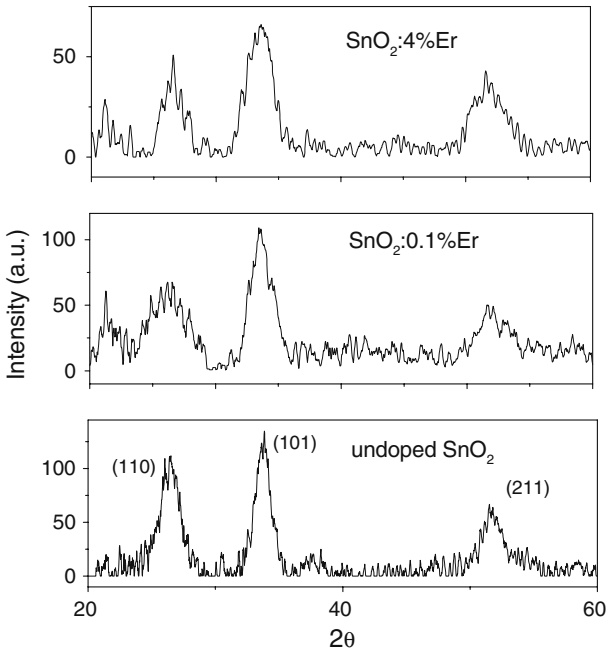

Fig. 4 X-ray diffraction data for undoped and Er-doped SnO_2 thin films, with the most evident directions labeled

shape profile, typical of small crystallite domain. Evaluating the average crystallite size from line broadening XRD pattern at (101) direction (Scherrer equation [21]), which is the most clearly defined peak in Fig. 4, one obtains values listed on Table 1.

It is quite clear from Table 1 that our hypothesis of electrical transport dominated by grain boundary scattering, used in the model proposed in Section ''Analyses of the decay of photoinduced conductivity'', is adequate since the average grain size is very small. Besides it can also be seen from Table 1 that the introduction of Er inhibits the grain growth, leading to lower mobility samples as the Er^{3+} concentration increases, in agreement with the previous discussion.

Conclusion

Erbium (Er^{3+}) presents acceptor like nature in SnO_2 thin films, which leads to high charge compensation, since undoped tin dioxide is originally an n-type material. It makes these films very resistive. From a theoretical data-fitting procedure, we conclude that Er^{3+} related centers present a thermally activated capture cross section and the decay of photoexcited conductivity is temperature and concentration dependent. Our model assumes the grain boundary scattering as dominant mechanism, which allows to obtain the quantity (E_{cap}–ϕ), which is 118 meV for SnO_2:4% Er and 70 meV for SnO_2:0.1% Er. We believe that the dominant scattering centers in these samples come from distinct centers. For SnO_2:0.1% Er the trapping are related to Er^{3+} centers located at lattice sites and for SnO_2:4% Er the capture centers are at grain boundary layer, since 4% of Er is well above the solubility limit.

The activation energy obtained from Arrhenius plot agrees with the quantity (E_{cap}–ϕ). Then the Arrhenius plot must be carefully used in samples with anoscopic grains, because the potential barrier at grain boundary (ϕ) becomes comparable to the thermally activated capture barrier (E_{cap}). The hypothesis of grain boundary scattering is in good agreement with X-ray diffraction data, since the evaluation of grain size from line broadening of XRD pattern yields nanoscopic grain dimensions.

The understanding of photo-induced electrical properties of Er-doped SnO_2 is essential towards a complete description of electroluminescent centers present in this material. We believe that this report will help to clarify the physics of Er-related centers envisaging its modulation and control to electroluminescent devices operation.

Table 1 Grain size estimation from XRD diffraction data for undoped and Er-doped SnO_2 thin films

Er concentration (mol%)	Average grain size (nm)(101) direction
0.0	6.02
0.1	5.18
4.0	3.53

Acknowledgements The authors wish to thank Prof. Sidney J. L. Ribeiro for all the help with technical set-up and very fruitful discussions, and Viviany Geraldo for the undoped SnO_2 sample. They also acknowledge CAPES, CNPq and FAPESP for financial support

References

1. Franzò G, Priolo F, Coffa S, Polman A, Carrera A (1994) Appl Phys Lett 64:2235
2. Fanevee PN, 'Haridon HL, Salvi M, Muotonnet D, de Guillo Y (1989) Electron Lett 25:718
3. Casero RP, Liorente AG, Y-Moll OP, Seiller W, Deforneau RM, Defornoeau D, Millon E, Perrière J, Goldner P, Viana B (2005) J Appl Phys 97:054905-1
4. Kenyon AJ (2002) Prog Quantum Electron 26:225
5. Zavada JM, Jin SX, Nepal N, Lin JY, Jiang HX, Chow P, Hertog B (2004) Appl Phys Lett 84:1061
6. Abello L, Bochu B, Gaskov A, Koudryavtsevaet S, Lucazeau G, Roumyantseva M (1998) Solid State Chem 135:78
7. Amma DSD, Vaidyan VK, Manoj PK (2005) Mater Chem Phys 93:194
8. Ray SC, Karanjai MK, Dasgupta D (1998) Surf Coatings Technol 102:73

9. Gonçaves RR, Ferrari M, Chiasera A, Montagna M, Morais EA, Scalvi LVA, Santilli CV, Messaddeq Y, Riveiro SJL (2002) J Metastab Nanocryst Mater 14:107
10. Morais EA, Scalvi LVA, Geraldo V, Scalvi RMF, Ribeiro SJL, Santilli CV, Pulcinelli SH (2004) J Eur Ceram Soc 24:1857
11. Morais EA, Scalvi LVA, Ribeiro SJL, Geraldo V (2005) Phys Stat Sol (A) 202:301
12. Simmons JG (1971) J Phys D 4:613
13. Ohring M (1992) The Materials Science of Thin Films. Academic Press, New York
14. Dobson TW, Scalvi LVA, Wager JF (1990) J Appl Phys 68:601
15. Scalvi LVA, Minami E (1993) Phys Stat Sol (A) 139:145
16. Shanth E, Dutta V, Banerjee A, Chopra KL (1981) J Appl Phys 51:6243
17. Zhang DH, Ma HL (1996) Appl Phys A 62:487
18. Morais EA, Ribeiro SJL, Scalvi LVA, Santilli CV, Ruggiero LO, Pulcinelli SH, Messaddeq Y (2002) J Alloys Comp 344:217
19. Geraldo V, Scalvi LVA, Morais EA, Santilli CV, Miranda PB, Pereira TJ (2005) J Eur Ceram Soc 25:2825
20. Powder Diffraction File (1983) Inorganic, vol 21, JCPDS, Swathmore
21. Cullity BD (1978) Elements of X-ray diffraction. Addison–Wesley Publ Comp, Reading Mass